

Removal of Spectro-Polarimetric Fringes by 2D Pattern Recognition

R. Casini,¹ P. G. Judge,¹ T. A. Schad,²

¹ *High Altitude Observatory, NCAR,¹P. O. Box 3000, Boulder, CO 80307-3000, U.S.A.*

² *Lunar and Planetary Lab, University of Arizona, Tucson, AZ 85721, U.S.A.*

ABSTRACT

We present a pattern-recognition based approach to the problem of removal of polarized fringes from spectro-polarimetric data. We demonstrate that 2D Principal Component Analysis can be trained on a given spectro-polarimetric map in order to identify and isolate fringe structures from the spectra. This allows us in principle to reconstruct the data without the fringe component, providing an effective and clean solution to the problem. The results presented in this paper point in the direction of revising the way that science and calibration data should be planned for a typical spectro-polarimetric observing run.

1. Introduction

The observation and interpretation of wavelength dependent polarization signals in spectral lines is the primary method for the diagnostics of anisotropic processes in astrophysical plasmas, such as those induced by the presence of deterministic electric and magnetic fields (e.g., Stenflo 1994; Landi Degl’Innocenti & Landolfi 2004; Casini & Landi Degl’Innocenti 2008; Trujillo Bueno 2010), or by plasma collisions with collimated beams of ions (e.g., Fujimoto 2008). At the same time, the depolarizing effects by isotropic collisions and by quasi-random electro-magnetic fields can yield information on the density of the plasma constituents, as well as important insights on the overall complexity of turbulent plasmas at diverse spatial and temporal scales (e.g., Casini, Manso Sainz, & Low 2009).

The amplitudes of polarization signals observed in astrophysical plasmas vary widely, ranging from the very small signatures ($\lesssim 10^{-3} I$, where I is the radiation intensity) typical of the weak-field modifications of scattering polarization by the Hanle effect (see, e.g., Landi Degl’Innocenti & Landolfi 2004), to large amplitudes ($\gtrsim 10^{-1} I$) induced by the Zeeman effect in the presence of strong magnetic fields, such as those found in sunspots. The weaker polarization signals are easily swamped by systematic errors associated with instrumental effects, which are often difficult to model to the level of precision (*polarization accuracy*) that is needed in order to isolate the true signals coming from the observed physical system. The calibration of this *instrumentally induced polarization*

¹The National Center for Atmospheric Research (NCAR) is sponsored by the National Science Foundation.

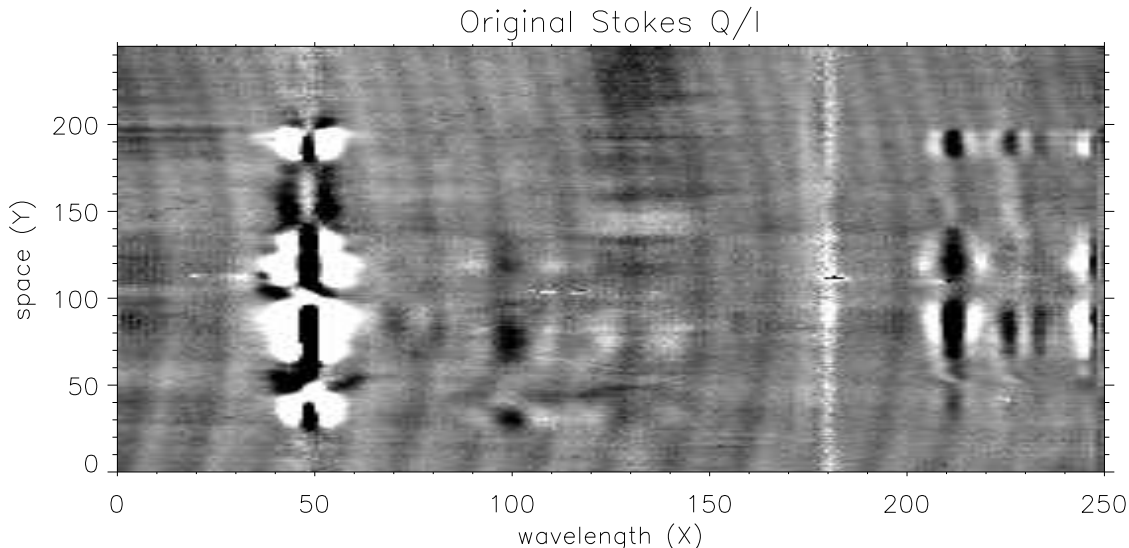


Fig. 1.— Example of spectro-polarimetric data, showing real spectral line polarization signatures superimposed to instrumental effects, including polarized fringes and detector noise. The abscissa is wavelength, while the ordinate is position along the instrument’s slit. The spectral range includes the line of Si I at 1082.7 nm (around $X = 50$), the two components of He I at 1083 nm (around $X = 100$ and $X = 130$), the telluric H_2O line (around $X = 180$), and the Ca I doublet at 1083.3 nm (approximately from $X = 210$ and $X = 230$).

is a difficult art. At the same time, the pursuit of ever finer spatial and temporal scales in the investigation of astrophysical plasmas puts continually growing demands on both sensitivity (i.e., signal-to-noise) and accuracy of polarimetric observations (e.g. Rimmele et al. 2008). Even higher demands are being made by the scientifically critical need to measure chromospheric magnetic fields (Judge 2010).

Polarized fringes are commonly found in spectro-polarimetric data. These are interference patterns that arise because of the presence of optical components (also including air) in a spectro-polarimeter, which have different refractive and/or birefringent properties. Such components include polarization modulators, polarizing beam-splitters, and any optical system where parallel optical interfaces may occur (e.g., interference filters, detector windows). These fringes have the appearance of more or less regular bidimensional patterns, often curved, which typically unfold along the spectral dimension of the data (see Fig. 1). We refer to review studies of polarized fringes (Semel 2003; Clark 2004) for a thorough description of this phenomenon. Here, we are interested exclusively with the treatment of this artifact during data reduction.

The treatment of polarized fringes has been a recurring problem for the reduction and analysis of spectro-polarimetric data. The state of the art is to attempt removal of these (and other) instrumental effects using Fourier methods or wavelet analysis (e.g., Rojo & Harrington 2006).

Fourier filtering has been successful at removing various types of data artifacts, when their range of spectral and/or spatial frequencies is clearly separated from that of the actual signal of the observed source (L. Kleint, private communication). Wavelet analysis attempts to identify the dominant frequencies and phases of the fringe pattern in a data frame, when the artifacts are not strictly periodic. Rojo & Harrington (2006) have developed a localized solution to fringe pattern reconstruction by employing two-dimensional wavelet transforms, which excel at tracking smooth variations in phase and amplitude of a periodic signal. The shape of a fringe pattern can be isolated in the wavelet space of individually transformed image rows, each row corresponding to a spatial point in the map. An inverse wavelet transform of the fringe space then can reconstruct the fringe pattern in the spatial domain. This can be a particularly powerful method for removing fringes in flat field images, but its application to object images (especially polarized spectral images) is complicated by the contribution of the targeted signal to the local wavelet transform.

Unfortunately, fringe patterns are seldom regular, having an intrinsic bidimensional structure, with variations of the amplitude, frequency, and phase, which can be significant in both the spectral and spatial dimensions (see Fig. 1). Often fringe patterns result from the combination of more than one component, and this combination can also vary smoothly across the dataset. In this case, a two-dimensional wavelet analysis of the observations is challenged by the need to treat every frame separately. In this paper, we propose instead that the identification and removal of polarized fringes might be better approached as a problem of pattern recognition.

Since polarized fringes typically arise within the spectro-polarimeter,² we expect their structure to be predominantly a function of the instrument configuration. Let us consider a scanning slit instrument. During the spatial scan of a given target, the instrument configuration is approximately fixed. We can expect that the polarized fringes will constitute an approximately time-independent pattern within that particular dataset, although there may be some dependence of the fringes’ appearance (in both amplitude and phase) on the polarization state of the light entering the spectro-polarimeter. As the spatial scan is acquired, the polarimetric signal of the target will then change over an approximately constant fringe background. Heuristically, an “orthogonality” exists between the true polarimetric signal that we wish to analyze and this “fixed” fringe background, as a consequence of the fact that the two sources of the line signals and of the background are largely uncorrelated. This suggests that the problem of identification and removal of polarized fringes should be approached as a problem of pattern recognition and feature extraction from a two-dimensional dataset. For this paper we decided to approach this problem using two-dimensional Principal Component Analysis (2D PCA; Yang et al. 2004). Other methods could potentially be adopted instead, which also have been used for the separation of signals from uncorrelated sources, such as the Independent Component Analysis (ICA; e.g., Jutten & Hérault 1991). We defer the study of some of these alternative methods for the problem of the identification and removal of

²A notable exception is represented by fringing that is caused by the polarization calibration optics, which may reside outside the spectro-polarimeter, often well upstream in the optical system of the telescope.

polarized fringes to future work.

The simple fact that spectral line signals and polarized fringe background are largely uncorrelated is central to the success of the PCA approach to the problem at hand. This concept is nicely summarized by Jolliffe (2002) in the Introduction to his book: “*The central idea of principal component analysis (PCA) is to reduce the dimensionality of a data set consisting of a large number of interrelated variables, while retaining as much as possible of the variation present in the data set. This is achieved by transforming to a new set of variables, the principal components (PCs), which are uncorrelated, and which are ordered so that the first **few** retain most of the variation present in **all** of the original variables.*”

Preliminary considerations on the problematics associated with PCA filtering of polarized fringes from Stokes profiles were already advanced in a study on *compressed sensing* of experimental data (Asensio Ramos & López Ariste 2010). In this work, we provide a novel and more in-depth investigation of the problem. In Sect. 2 we summarize the main ideas behind two-dimensional PCA, and show how these can be applied to the specific problem of the removal of polarized fringes from spectro-polarimetric data. In Sect. 3, we describe the observations from which the datasets used for the testing of the method were extracted. In Sect. 4 we present various examples of application of the method to the datasets previously described, and comment on the quality and reproducibility of the results. Finally, in our concluding remarks, we briefly discuss possible observation and data calibration strategies that could help fully realize the potential of the proposed method.

2. Two-dimensional Principal Component Analysis

The theory behind PCA is well established (Pearson 1901; Jolliffe 2002). PCA has been successfully applied to a related but different problem of the inversion of spectro-polarimetric data for the inference of the thermodynamic and magnetic structure of the solar atmosphere (Rees et al. 2000; Socas-Navarro et al. 2001; López Ariste & Casini 2002; Casini, Bevilacqua, & López Ariste 2005; Casini et al. 2009). In this application, PCA is used to identify an orthogonal set of spectral *eigenfeatures* characteristic of a given line formation model in a magnetized atmosphere. One then determines the principal components (projections) of the observed spectra on this orthogonal eigenbasis, and searches within a pre-calculated database of model profiles for the closest set of components to the observed set. The quality of the inversion is estimated by the “PCA distance” between the observed and inverted points in the PCA-component space. This distance is akin to the usual χ^2 estimator for a non-linear least-squares fit. In this special application, PCA then produces a best fit of the observed Stokes profiles as a function of wavelength. PCA is able to capture the structures of the observed profiles that correspond to the physical model used for the construction of the inversion database. Systematic errors introduced by the instrument, or by physical mechanisms not included in the model, cannot be captured by the PCA inversion, and consequently they tend to increase the inversion noise (i.e., the PCA distance). Because every spatial point is emitting incoherently from all the other points in the map, the spectro-polarimetric

inversion must be performed separately for each spatial point of the scan.

The application of PCA to our problem is instead subject to rather different constraints. First of all, polarized fringes are typically very hard to model, and their appearance – such as frequency, phase, as well as shape – can be very specific of the particular observing and instrumental setup, and may change significantly between different observations. Therefore, rather than creating a model-based database of fringes to compare with the observations, one should extract the PCA eigenfeatures of the fringe pattern directly from the observed data. Another substantial difference is that the treatment of fringes is better done simultaneously on the entire detector frame, because of the intrinsic bidimensional nature of these instrumental artifacts. The correct approach should then be analogous to the one adopted in the application of PCA to face recognition.

To further proceed, we need to choose one among the various PCA algorithms that have been developed for face recognition (Kirby & Sirovich 1990; Turk & Pentland 1991; Yang et al. 2004). The 2D PCA algorithm proposed by Yang et al. (2004) appears to outperform other approaches, and so we selected it for our problem. We summarize here below the fundamental ideas of this algorithm.

We indicate with \mathbf{A}_i , for $i = 1, \dots, N$, a set of images (e.g., the sequential series of the frames in a spectro-polarimetric map), each represented by a $m \times n$ matrix. From these, we can create the $n \times n$ covariance matrix

$$\mathbf{C} = \frac{1}{N} \sum_{i=1}^N (\mathbf{A}_i - \bar{\mathbf{A}})^T (\mathbf{A}_i - \bar{\mathbf{A}}), \quad \bar{\mathbf{A}} = \frac{1}{N} \sum_{i=1}^N \mathbf{A}_i. \quad (1)$$

It is demonstrated (e.g., Jolliffe 2002) that the *optimal* set of projection vectors for the decomposition of the data, for the purpose of extracting its *principal components*, is represented by the n eigenvectors of the covariance matrix. These eigenvectors can conveniently be determined by performing the *singular value decomposition* (SVD) of \mathbf{C} . The result is a set of mutually orthogonal, n -dimensional vectors, \mathbf{U}_j , with $j = 1, \dots, n$, which can be interpreted as the column vectors of a $n \times n$ orthogonal matrix $\mathbf{U} = \{\mathbf{U}_1, \dots, \mathbf{U}_n\}$. It is customary to order the set of eigenvectors $\{\mathbf{U}_i\}_{i=1, \dots, n}$ (the *eigenfeatures*) according to the decreasing amplitude of the associated singular values, σ_i , so that \mathbf{U}_1 corresponds to the singular value with the largest amplitude. In turn, the singular values can be interpreted as the weights of the corresponding eigenfeatures in their contribution to the dataset $\{\mathbf{A}_i\}_{i=1, \dots, N}$. The set $\{\mathbf{U}_i\}_{i=1, \dots, n}$ is complete, and thus forms a basis for the dataset $\{\mathbf{A}_i\}_{i=1, \dots, N}$.

Once the basis $\{\mathbf{U}_i\}_{i=1, \dots, n}$ has been determined, the set of *principal components* (or projections) for each of the elements of the dataset $\{\mathbf{A}_i\}_{i=1, \dots, N}$ is

$$\mathbf{V}_i = \mathbf{A}_i \mathbf{U}, \quad i = 1, \dots, N. \quad (2)$$

We note that each \mathbf{V}_i is a $m \times n$ matrix, which can be thought of as the set of m -dimensional column vectors, $\{\mathbf{V}_{i,j}\}_{j=1, \dots, n}$, such that

$$\mathbf{V}_{i,j} = \mathbf{A}_i \mathbf{U}_j, \quad i = 1, \dots, N, \quad j = 1, \dots, n. \quad (3)$$

Since \mathbf{U} is an orthogonal matrix with unit determinant, eq. (2) can be immediately inverted,

$$\mathbf{A}_i = \mathbf{V}_i \mathbf{U}^T = \sum_{j=1}^n \mathbf{V}_{i,j} \mathbf{U}_j^T, \quad i = 1, \dots, N. \quad (4)$$

This equation represents the algorithm for the reconstruction of the image \mathbf{A}_i from its PCA component matrix, \mathbf{V}_i , and the PCA eigenbasis \mathbf{U} . In particular, any truncation of the summation on the left of eq. (4), up to some index $j = j_{\max} < n$, will provide an approximate reconstruction of the original image,

$$\tilde{\mathbf{A}}_i = \sum_{j=1}^{j_{\max}} \mathbf{V}_{i,j} \mathbf{U}_j^T. \quad (5)$$

If the image set is characterized by a low degree of entropy (that is, a high level of ordering – like for the image of an object, or, in our case, the Sun’s line spectrum between two fixed wavelengths), the amplitudes of the singular values drop very fast – typically, by several orders of magnitude within the first few eigenfeatures. This implies that the information content of the data is practically confined within a set of eigenfeatures which is much smaller than the complete set,³ which, on the other hand, will also contain information on less significant and/or more random features of the images, including noise.

Equation (1) shows that a perfectly constant background affecting all images \mathbf{A}_i is completely removed from the expression of the covariance matrix \mathbf{C} . In such an ideal case, the eigenvectors $\{\mathbf{U}_i\}_{i=1,\dots,n}$ constitute an optimal set of projection vectors for the relevant signal in the data, but not for the background. One should then expect to be able to reconstruct the signal to any degree of precision (including noise), while leaving the constant background out. This, of course, is never the case with real spectro-polarimetric data. Residual fringing is going to be present in the covariance matrix, and this ultimately affects the ability to reconstruct spectral signals that happen to be co-located with the fringes, and with comparable amplitudes.

Note that the form of eq. (1) implies that the bidimensional dataset is summed (*contracted*) over the m rows of the differential images $(\mathbf{A}_i - \bar{\mathbf{A}})$. Alternatively, we could have defined the covariance matrix as the average of the products $(\mathbf{A}_i - \bar{\mathbf{A}})(\mathbf{A}_i - \bar{\mathbf{A}})^T$ over the dataset, implying a contraction over the n columns of the differential images. In PCA applications to face recognition it typically is irrelevant whether the PCA covariance matrix is computed by contracting the bidimensional data over the X - or the Y -axis. For the analysis of Stokes maps, instead, the spectral dimension (conventionally identified in this work with the X -axis) represents a privileged coordinate. The reason is two-fold. First of all, it is essential for our problem that we preserve the distinction among the different spectral features in a Stokes map. In fact, because different spectral lines may be formed under very diverse atmospheric conditions, and have distinct thermal and magnetic diagnostic properties, it is important that their characteristics be kept distinct in

³Incidentally, this property provides a convenient means for data compression.

the PCA decomposition of the Stokes data. If we were instead to contract the data along the spectral dimension, the diagnostic information from all spectral lines would be merged together. Furthermore, preserving the spectral dimension in the PCA decomposition of a Stokes map allows us to isolate a specific subinterval of the spectral domain, if needed. The second argument is that polarized fringes tend to occur preferentially along the spectral dimension. Again, if we were to contract the data over wavelength, the spectral information of the polarized fringes would be completely merged with that from the spectral lines. The immediate consequence is that each of the PCA eigenfeatures would then always contain the information from both spectral lines and polarized fringes, making the filtering out of fringes impossible. All examples shown in the following discussion rely on the preservation of the spectral information of the Stokes map in the PCA decomposition. For this reason, we adopt the definition of the covariance matrix given by eq. (1).

3. Observations

Spectro-polarimetric observations of an active region near the solar limb were taken on September 22, 2011 with the Facility Infra-Red Spectro-polarimeter (FIRS; Jaeggli et al. 2010) and the Interferometric BIdimensional Spectrometer (IBIS; Cavallini 2006; Reardon & Cavallini 2008). Both instruments are deployed at the Dunn Solar Telescope (DST) of the National Solar Observatory on Sacramento Peak (NSO/SP, Sunspot, NM). FIRS was used in a single-slit, dual-beam mode, with the slit oriented tangentially to the solar limb. The 75''-long projected slit was scanned across the solar image, in 70 steps of 0.65'', to produce images in four polarimetrically modulated states, S_i . The spectral range of the observations spanned from 1081.93 to 1085.01 nm.

The data were reduced using software originally developed by S. Jaeggli (Jaeggli 2011) and modified by one of the authors (TS). The data reduction followed the standard procedures: 1) correction for non-linearities of the detector; 2) subtraction of dark frames; 3) division by flat fields; 4) co-registration of the two beams, including corrections for image rotation; 5) polarization calibration; 6) de-modulation of the signals S_i to convert them into the corresponding Stokes parameters I , Q , U , and V . Special care was taken to acquire flat fields before and after the scans analyzed here, which were then linearly interpolated in time before being applied to the science data. This flat-field correction eliminated the dominant part of the signal contributed by the polarized fringes. However, there remained residual fringes and some other detector artifacts in the processed data. The method proposed here for the identification and removal of fringes has been applied to these reduced data.

4. 2D PCA of Stokes spectra with polarized fringes

As we anticipated in both Sects. 1 and 2, the ability of PCA to isolate a background pattern within a dataset depends critically on how constant the appearance of the background pattern is

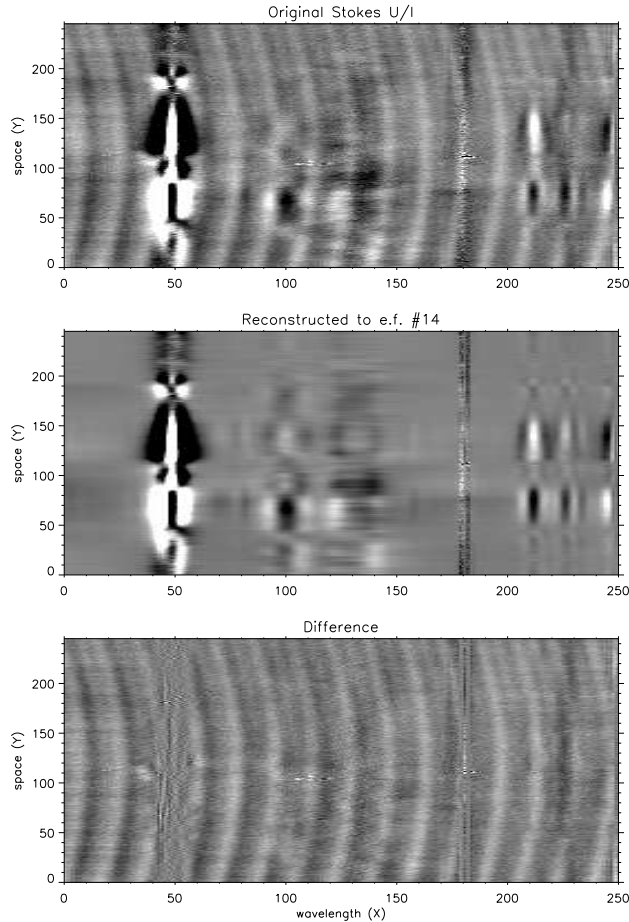


Fig. 2.— Example of PCA filtering of polarized fringes from a Stokes- U spectrum in the wavelength region of He I 1083 nm. The He I triplet spans approximately between $X = 90$ and $X = 150$ on the horizontal axis. The top panel shows the original data, the middle panel the PCA reconstructed data (using the first 14 PCA eigenfeatures), and the bottom panel shows the difference of the two. We see how most of the large-scale fringes have been taken out in the PCA reconstruction, revealing more clearly “real” solar spectral features.

throughout the dataset. In particular, to eliminate any unwanted artifact from the scientifically relevant data, it is important that the realizations of the relevant signals throughout the dataset be as varied as possible (and ideally vanish for a *statistically significant* number of frames), while the pattern of the artifact should remain practically constant. This allows PCA to “recognize” the signals and the background pattern as originating from uncorrelated sources, and ultimately to isolate the pattern into an “orthogonal” subspace with respect to the signals. *This is the fundamental property enabling a PCA reconstruction of the scientific data that excludes the artifact.*

An application of the concepts presented so far is illustrated by Fig. 2, showing the Stokes- U spectrum in the wavelength region of He I 1083 nm, taken from the observations presented in

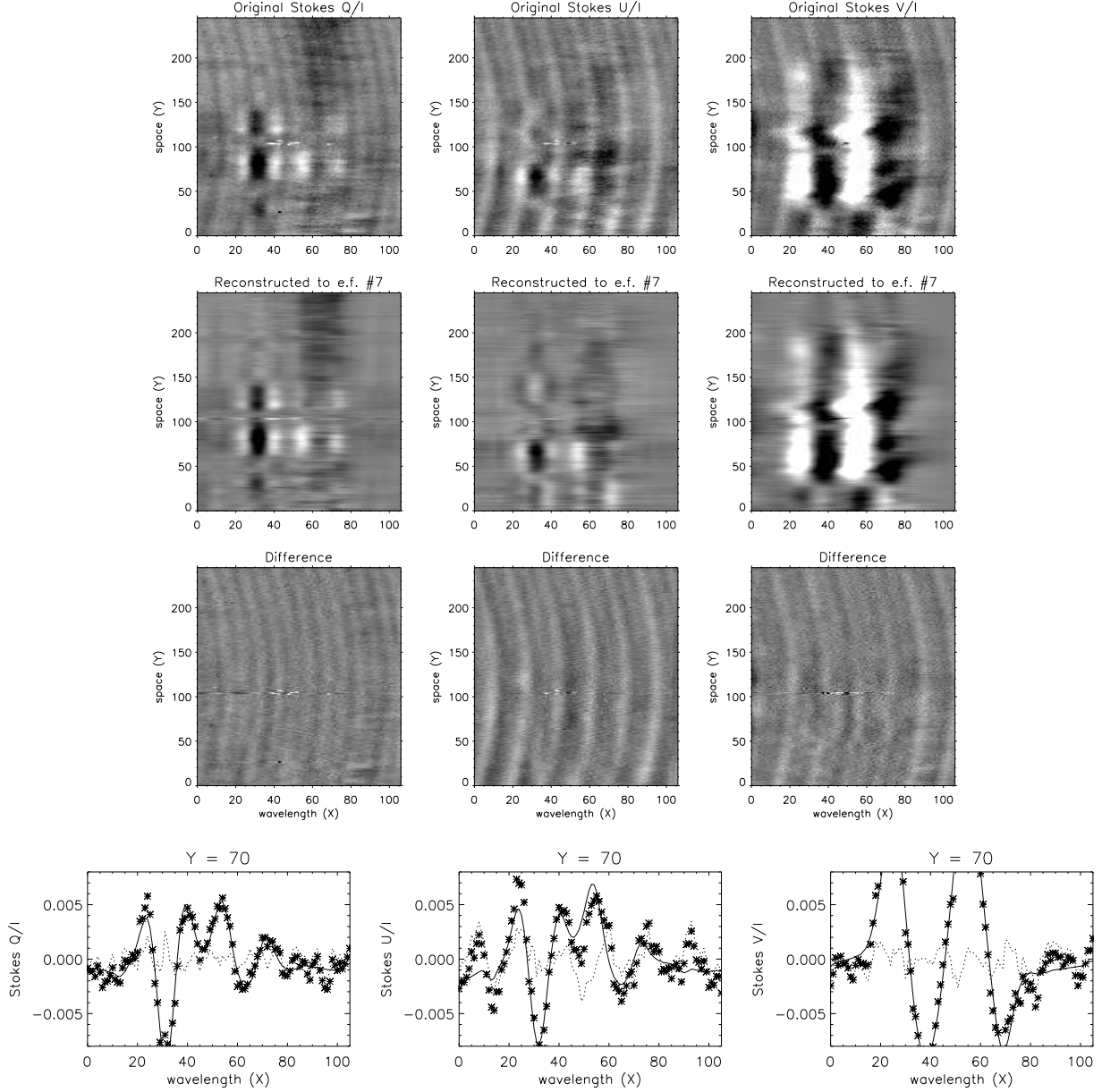


Fig. 3.— Same dataset as in Fig. 2, but with the PCA filtering applied only to the spectral region encompassing He I 1083 nm. The avoidance of the strong signatures of the Si I line and the H_2O atmospheric line allows for an efficient removal of the fringe pattern already with half the number of eigenfeatures as used for Fig. 2. The bottom panels show the Stokes profiles for the spatial point $Y = 70$. Star symbols show the data, the continuous line shows the reconstructed data, and the dotted line the difference of the two.

Sect. 3. This particular spatial scan encompasses a strongly magnetized active region with an overlying filament, as well as a portion of the quiet Sun. In these plots, the spectral dispersion (wavelength) is along the horizontal axis, and the spatial dimension is along the vertical axis. From left to right, we recognize the spectral features of the Si I line at 1082.7 nm, the He I triplet at 1083 nm, an H₂O telluric absorption line, and the Ca I doublet at 1083.3 nm (the leftmost signal is part of the Na I triplet at 1083.5 nm).

The Si I line shows a dominant signal in all frames of the map, with an average central depth of about 0.5 in intensity, and polarization levels typically between 10 and 20%. The H₂O telluric line also shows some polarization, at the level of 1% for linear polarization and a few times smaller for circular polarization. This must be an instrumental artifact, indicating a problem with the demodulation of the polarized signals into the Stokes vector, likely due to incorrect flat-fielding caused by the non-linearities of the FIRS IR detector (Jaeggli 2011). Because of this, the H₂O line also appears in all the frames of the Stokes map. The polarized fringes are also visible as curved structures spanning the wavelength domain. For the example of Fig. 2, we performed a PCA decomposition of the Stokes-*U* map, consisting of 45 slit positions over the solar disk, and reconstructed the data for one particular slit position, using only the first 14 eigenfeatures out of the 250 total (in our decomposition, the number of eigenfeatures equals the number of wavelength points in the scan; see Sect. 2). We note how the signals are well captured by the PCA reconstruction, while the fringes are “confined” within the orthogonal subspace corresponding to eigenfeatures larger than #14, almost everywhere in the spectral domain of the map. The spectral ranges of the Si I and H₂O lines are an exception, precisely because of their strong polarization signals appearing in all frames of the map, which prevents the PCA decomposition from separating these signals from the background fringes. In other words, at these particular wavelengths, PCA is unable to conclude that the spectral line signal and the fringes are uncorrelated.

Figure 3 shows instead the results of the PCA decomposition applied to a restricted set of wavelengths, encompassing just the He I triplet. The three columns show the intensity-normalized *Q*, *U*, and *V* Stokes parameters. Like in the previous example, PCA decomposition is able to isolate the fringes, because of the much more diverse appearance of the He I polarization signals in the map. However, we also note how the fringe background can be isolated and removed already using a PCA reconstruction that takes into account only half of the eigenfeatures that were used for Fig. 2. This is not surprising, since the low-order PCA eigenfeatures are always dominated by the structures that produce the largest variance in the data, and thus the strong signals of the Si I line, as well as the sharp H₂O line, occupy exclusively the first two eigenfeatures in the PCA decomposition of the full-range spectral maps depicted in Fig. 2, while the weakest signals of the He I triplet and the polarized fringes only show up in later orders. In the case of the spectral maps of Fig. 3, instead, the variance of the data is dominated by the He I signals, which therefore appear in the PCA decomposition already in the lowest order. In fact, increasing the number of eigenfeatures in the reconstruction of the examples of Figs. 2 and 3 does not improve the quality of the fringe removal, but rather the fringe pattern starts leaking back into the reconstructed image.

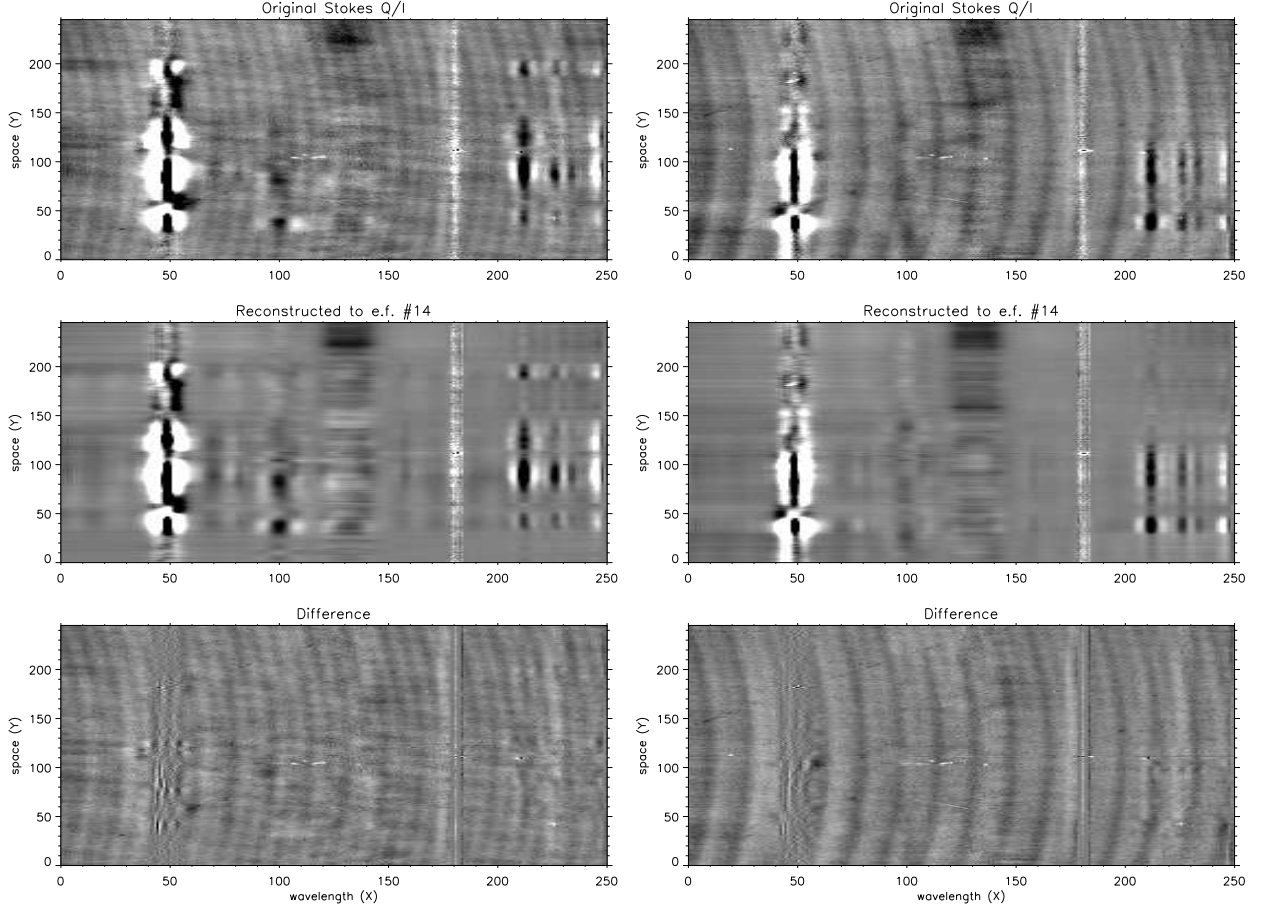


Fig. 4.— PCA reconstruction of two different Stokes- Q scan steps from the same dataset, showing how the fringe pattern can appear with distinct frequencies at different positions in the map. The PCA decomposition in this case is able to identify the two frequencies in the dataset, and subtract the proper combination of the respective contributions.

Again, this is due to the imperfect subtraction of the fringe background in the creation of the covariance matrix of the data.

In the datasets that we have analyzed from the FIRS instrument, the fringe patterns of a spectro-polarimetric map seem to occur always with one frequency and its first harmonic, as well as with various combinations of the two, although seemingly with nearly constant phases throughout the map. Apparently, PCA is able to identify the right combinations of these two basic fringe patterns and remove them from the spectral line signal (see Fig. 4). As long as a statistically significant number of samples of the recurring frequencies and phases of the fringes are present in a given observation, without contamination from the data (i.e., with vanishing spectral signals), we can reasonably assume – and is demonstrated in practice – that the PCA decomposition will be able to identify those characteristics, and their contributions to any given frame of the map.

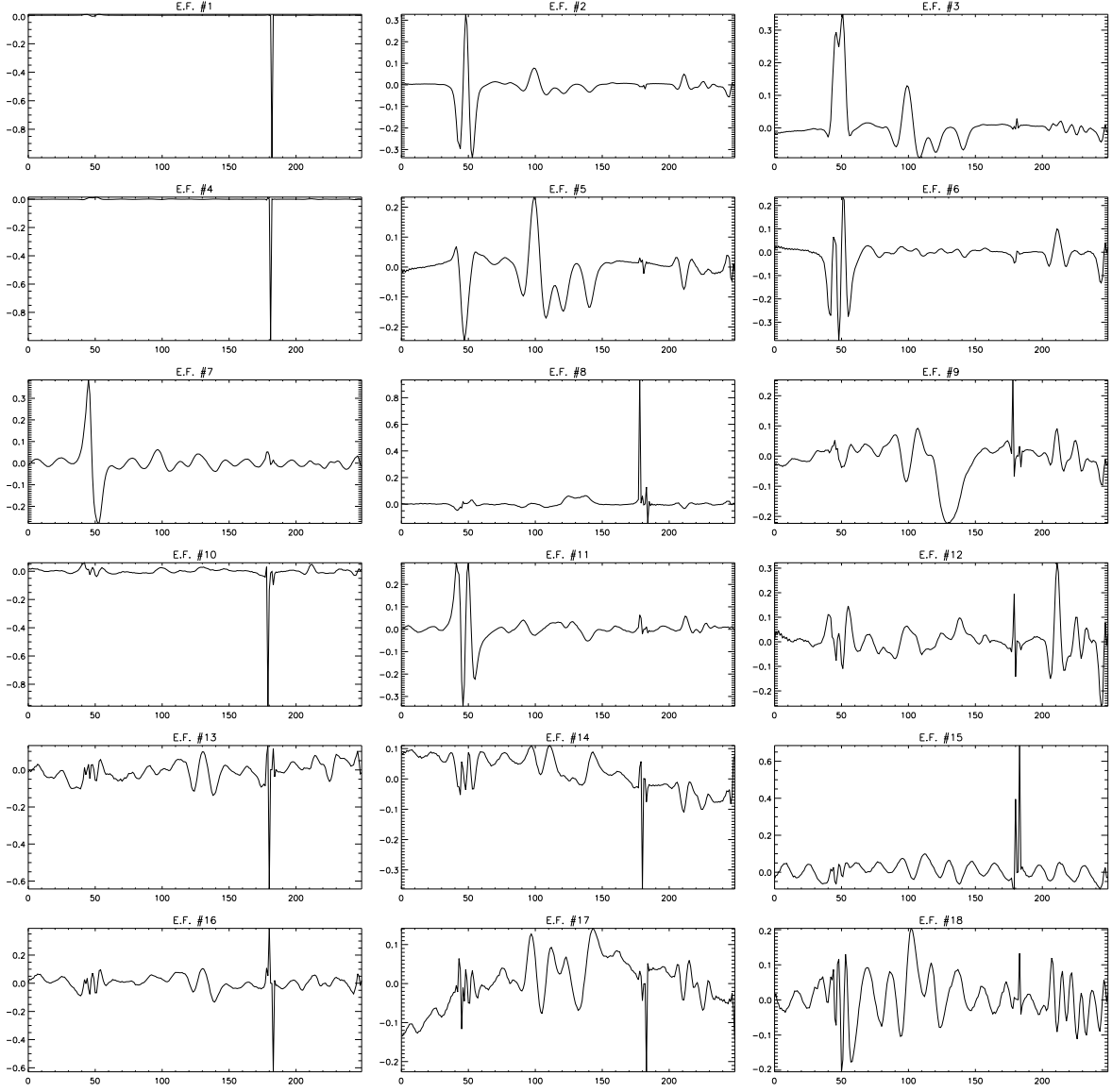


Fig. 5.— The first 18 basis eigenfeatures \mathbf{U}_i for the Stokes- Q dataset from which the two scan steps of Fig. 4 were taken.

On the other hand, if the frequency and/or phase of polarized fringes vary continually with the map step of a given dataset, then we can expect that the removal of fringes by PCA cannot be successfully accomplished within that individual dataset.

We conclude this section by commenting on possible strategies to decide the order of truncation of the PCA reconstruction that is needed for a specific dataset, since ideally one would like to devise some type of automated procedure for fringe removal from Stokes data.

The data that we have analyzed in this work were acquired during observations that were not specifically prepared to optimize the removal of polarized fringes. Therefore, the information content of fringes varies greatly between different datasets. As we have demonstrated, this affects both the quality of the fringe removal, as well as the number of PCA eigenfeatures that must be retained in order to attain the best compromise between fringe removal and preservation of the original spectral line signals. Because of this, there is some degree of *subjectivity* in the truncation of the PCA eigenfeature expansion. We have already shown how clipping out strong signals from the spectral range that is to be analyzed in terms of principal components allows to retain a smaller number of expansion orders.

On the other hand, in the data presented here, the spectral information of the Stokes line profiles is never completely “orthogonal” to that of the polarized fringes. In addition, the amplitude of the fringes is typically of the same order of magnitude as the Stokes signals of the He I triplet that we want to refine. Thus, many of the eigenfeatures that contribute to the fringe pattern across a dataset will also contain information on the line signals (such as velocity shifts and asymmetries), which may be critical for the science. Under these conditions, the truncation of the PCA reconstruction expansion still requires human oversight, unfortunately, and so can hardly be automated.

Beside truncation of the PCA expansion in data reconstruction, a related issue is that of order selection, that is, the retaining or dropping of critical eigenfeatures that work in favor of the preservation of the line signal simultaneously with the removal of polarized fringes and other artifacts. A cursory look at the structure of the basis eigenfeatures \mathbf{U}_i and of the *subimages* $\mathbf{V}_{*,i}\mathbf{U}_i^T$ that contribute to a given scan step of the dataset (cf. eq. [4]) is often very helpful to determine which order contains relevant spectral information, and which one instead can be dropped in order to remove the fringe background without critical loss of science data.

To illustrate this idea, Fig. 5 shows the first 18 eigenfeatures for the dataset from which the two scan steps of Fig. 4 were taken. We see at once some notable characteristics of this basis subset. The eigenfeatures #1 and #4 are completely dominated by the strong, sharp spectral signature of the H₂O line, while their contribution to the He I spectral range is effectively zero. The polarized fringes start appearing already in the eigenfeature #7, overlapped with a strong antisymmetric (i.e., velocity-type) component of the Si I line. Evidently the eigenfeature #15 is also completely dominated by fringes in the He I region. The eigenfeatures #14 and #17 do not tend to zero at the boundary of the spectral range. Likely this is caused by a residual gradient over the detector’s frame after flat-fielding, which could affect a proper collocation of the continuum level of the spectrum. With the exception of #7, the first eight eigenfeatures of Fig. 5 appear to be completely clear of the fringe background, only contributing to the line spectral signal that is relevant for science. All the successive eigenfeatures show instead some mixing of line spectra and fringes. Elimination of these eigenfeatures will inevitably determine some loss of science data, although this may occur at a level which lies below the target sensitivity of a particular observation.

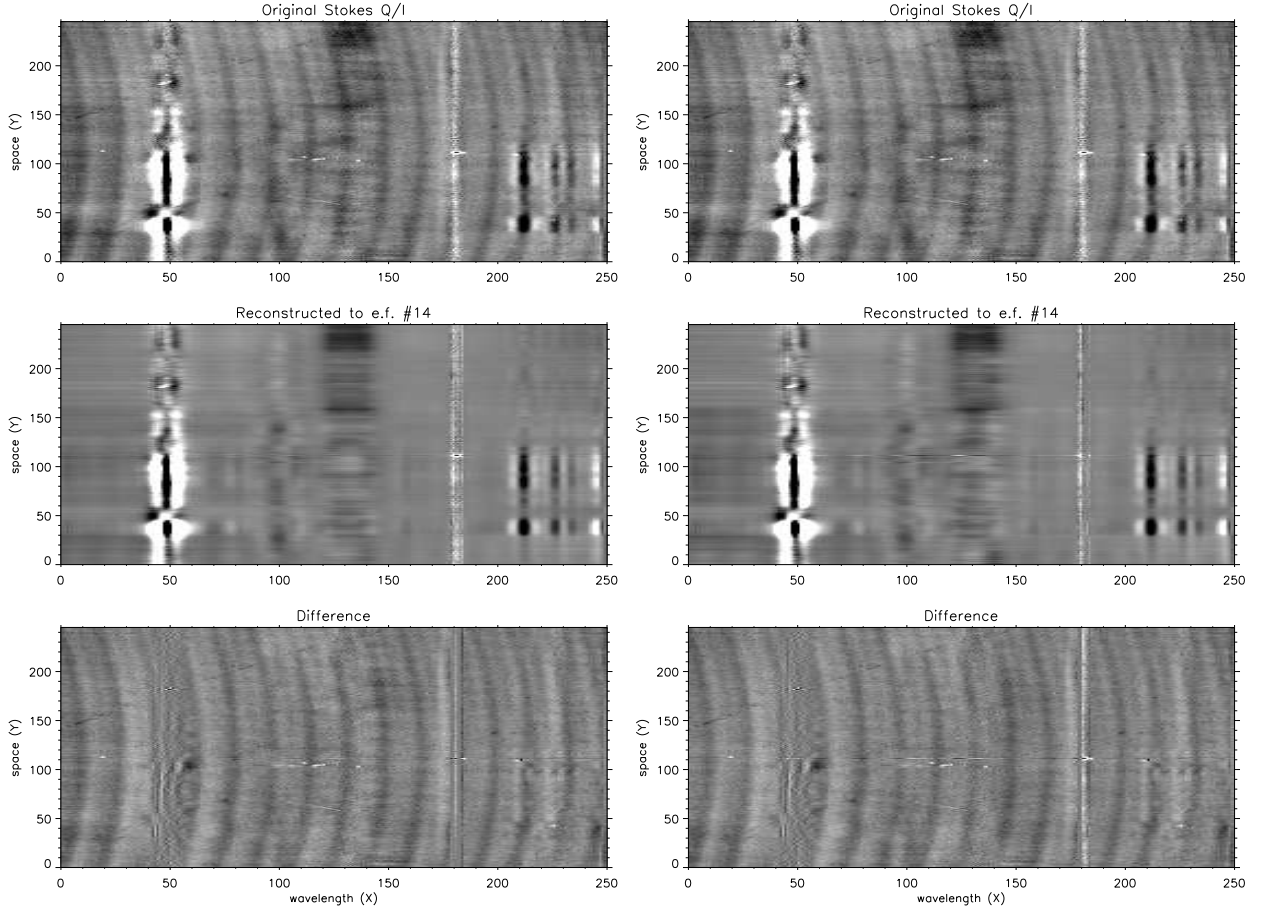


Fig. 6.— Different PCA reconstructions of the same Stokes- Q scan step; *left*: using the full set of the first 14 eigenfeatures; *right*: reconstructing the data by dropping the subset $\{1, 4, 14\}$ of eigenfeatures, and adding instead the subset $\{16, 18\}$. We note how the added eigenfeatures improve the reconstruction of the He I spectral data, while the quality of the fringe removal is preserved.

Figure 6 illustrates an application of this strategy of order selection. The left side shows the same Stokes- Q scan step used also for Fig. 4 (right side). The PCA reconstruction of the data implements the lowest 14 eigenfeatures in the PCA decomposition of the entire Stokes- Q map. This order of truncation does a good job at removing the polarized fringes, however it also appears to clip some of the finer spectral and spatial information in the He I triplet from the reconstructed data. This is noticeable, for example, in the appearance of the dark absorption feature located approximately at $Y = 155$, in the red component of He I 1083 nm (spanning approximately between $X = 120$ and $X = 140$). The reconstructed data shown on the right side of the figure is a modification of the PCA expansion used for the left side example, which was based on the characteristics of the eigenfeatures described above. The subset $\{1, 4, 14\}$ was removed from

the truncated PCA expansion, while we added the subset $\{16, 18\}$. Such operation indeed helped reducing the H_2O spectral signature from the scan. It was also able to capture more of the spectral and spatial complexity of the He I triplet, while at the same time preserving the quality of the removal of the polarized fringes.

5. Conclusions

The problem of the identification and removal of instrumental artifacts, such as polarized fringes, from spectro-polarimetric maps lends itself naturally to a treatment by pattern recognition methods, e.g., Principal Component Analysis (PCA). In this paper, we have presented the 2D PCA algorithm of Yang et al. (2004), which appears to outperform other PCA strategies in the tests of the authors of that work.

However, it is interesting to comment briefly also on the more traditional implementation of PCA to face recognition (Turk & Pentland 1991). In this alternate approach, each $m \times n$ image matrix \mathbf{A}_i is rearranged into a $(m \times n)$ -vector \mathbf{B}_i . The dataset of N images can then be represented by the $(m \times n) \times N$ matrix $\mathbf{B} = \{\mathbf{B}_i\}_{i=1, \dots, N}$, and the PCA covariance matrix is then built as

$$\mathbf{C} = \frac{1}{N} \sum_{i=1}^N (\mathbf{B}_i - \bar{\mathbf{B}})^T (\mathbf{B}_i - \bar{\mathbf{B}}), \quad \bar{\mathbf{B}} = \frac{1}{N} \sum_{i=1}^N \mathbf{B}_i. \quad (6)$$

We note that \mathbf{C} so defined is an $N \times N$ matrix, and that both the spatial and spectral dimensions of the original images \mathbf{A}_i have been contracted in order to compute it. This approach has the notable advantage of producing eigenfeatures that resemble the original images (see Turk & Pentland 1991, for details), which provide a direct visual aid for the selection of the orders that isolate the spectral data from the fringe background. On the other hand, the high level of data compression tends to produce a much slower convergence of the PCA reconstruction series than for the 2D PCA algorithm. The alternative of using the products $(\mathbf{B}_i - \bar{\mathbf{B}})(\mathbf{B}_i - \bar{\mathbf{B}})^T$ for the definition of \mathbf{C} (see also Sect. 2) would preserve both spatial and spectral information of the covariance of the original dataset. On the other hand, this would often create a matrix that is too big to be diagonalized efficiently for the typical values of the image dimensions, m and n . That is why the 2D PCA algorithm appears more suitable for our problem, despite the fact that the order selection may be more cumbersome with this approach. We defer a more detailed study of the potential and limitations of the traditional PCA approach to future work.

The strategy to make PCA succeed in the removal of polarized fringes from spectro-polarimetric data is ideally to guarantee the presence in a dataset of widely diverse realizations of a line's polarization profiles over a practically time-independent fringe background. In fact, this determines the condition of non-correlation between the spectral signal and the polarized fringes, which is at the very basis of the working concept of PCA (Jolliffe 2002).

For the He I 1083 nm data presented in this work, this condition is often met, and as expected

PCA manages to separate rather well the spectral line information from the fringe background. The Si I line is always prominent in the solar intensity spectrum. However, this should not always be the case for polarization, e.g., for quiet-Sun observations. So one can hope that the same strategy will work with that line as well, at the condition that a sufficient diversity of polarization signals over the fringe background can be acquired during an observation. In the active-region data that we have analyzed, instead, the polarization signals of the Si I line are always typically at the level of 10-20% for both linear and circular polarization, and thus the subtraction of the fringe background in that spectral range fails consistently. This problem is greatly mitigated by the fact that the typical amplitude of the fringes is relatively small ($\sim 0.2\%$) in our data, compared to the observed amplitudes of the Si I polarization, and so the polarization profiles of the line are not significantly affected by the fringe background.

The results presented in this paper point in the direction of revising the way that the acquisition of science and calibration data should be planned for a typical spectro-polarimetric observing run. Looking at different targets on the quiet Sun, while maintaining the same configuration of the spectrograph in order to preserve the stationarity of the fringe background, could turn out to be a fundamental addition to all observing programs. Lamp flat fields may also be an important tool for “fringe calibration”, as they could be used to augment the set of fringe data de-voided of spectral line signals for the purpose of “training” the PCA in the identification of fringes. Of course, these lamp flats should ideally be taken under the same optical configuration of the spectrograph as used for a given observation, which may not always be possible.

The authors enjoyed several stimulating discussions with A. López Ariste (THÉMIS-CNRS, France) and A. Asensio Ramos (IAC, Spain) on the problem of removal of polarized fringes by PCA and other methods. They are also grateful to HAO colleagues L. Kleint and R. Centeno Elliot, D. Elmore (NSO), and J. Stenflo (ETH, Switzerland), for helpful comments.

REFERENCES

- Asensio Ramos, A., & López Ariste, A. 2010, *A&A*, 509, 49
- Casini, R., Bevilacqua, R., & López Ariste, A. 2005, *ApJ*, 622, 1265
- Casini, R., & Landi Degl’Innocenti, E. 2008, *Astrophysical Plasmas*, in *Plasma Polarization Spectroscopy*, eds. T. Fujimoto & A. Iwamae (Springer: Berlin), 247
- Casini, R., López Ariste, A., Paletou, F., Léger, L. 2009, *ApJ*, 703, 114
- Casini, R., Manso Sainz, R., & Low, B. C. 2009, *ApJ*, 701, L43
- Cavallini, F. 2006, *Sol. Phys.*, 236, 415
- Clark, D. 2004, *J. Opt. A*, 6, 1036

- Fujimoto, T. 2008, Collision Processes, in Plasma Polarization Spectroscopy, eds. T. Fujimoto & A. Iwamae (Springer: Berlin), 91
- Jaeggli, S. A., Lin, H., Mickey, D. L., Kuhn, J. R., Hegwer, S. L., Rimmele, T. R., and Penn, M. J. 2010, Mem. SAIt, 81, 763
- Jaeggli, S. A. 2011, PhD Thesis, University of Hawaii
- Jolliffe, I. T. 2002, Principal Component Analysis, 2nd ed. (Springer: New York)
- Judge, P. G. 2010, Mem. SAIt, 81, 543
- Jutten, C., & Hérault, J. 1991, Signal Process., 24, 1
- Landi Degl’Innocenti, E., & Landolfi, M. 2004, Polarization in Spectral Lines (Kluwer: Dordrecht)
- López Ariste, A., & Casini, R. 2002, ApJ, 575, 529
- Kirby, M., & Sirovich, L. 1990, IEEE Trans. PAMI, 12, 103
- Pearson, K. 1901, Phil. Mag., 2, 559
- Reardon, K. P., & Cavallini, F. 2008, A&A, 481, 897
- Rees, D. E., López Ariste, A., Thatcher, J., & Semel, M. 2000, A&A, 355, 759
- Rimmele, T., & the ATST Team 2008, AdSpR, 42, 78
- Rojo, P. M., & Harrington, J. 2006, ApJ, 649, 553
- Semel, M. 2003, A&A, 401, 1
- Socas-Navarro, H., López Ariste, A., & Lites, B. W. 2001, ApJ, 553, 949
- Stenflo, J. O. 1994, Solar Magnetic Fields (Kluwer: Dordrecht)
- Trujillo Bueno, J. 2010, Recent Advances in Chromospheric and Coronal Polarization Diagnostics, in Magnetic Coupling between the Interior and Atmosphere of the Sun, Proc. Astrophysics and Space Science, eds. S. S. Hasan & R. J. Rutten (Springer: Berlin), 118
- Turk, M. A., & Pentland, A. P. 1991, JoCN, 3, 71
- Yang, J., Zhang, D., Frangi, A. F., & Yang, J.-Y. 2004, IEEE Trans. PAMI, 26, 131